Experimental Astronomy (2025) 60:16
https://doi.org/10.1007/s10686-025-10024-w

RESEARCH

DMD-based Multi-Object Spectrograph (D-MOS): AIV and first light results

Sriram S[1,2] · Vineeth Valsan[1] · Remya B. S[2] · Subramaniam A[2] · Maheswar G[2]

Received: 17 June 2025 / Accepted: 26 August 2025 / Published online: 8 October 2025

Abstract

A Digital Micromirror Device (DMD)-based Multi-Object Spectrograph (D-MOS) with an integrated imager has been developed. The optical performance of the MOS is evaluated through comprehensive laboratory calibration and on-sky observations using the 1.3-meter J.C. Bhattacharya (JCB) Telescope at the Vainu Bappu Observatory (VBO). The system is designed to assess the viability of using a DMD as a programmable slit mechanism for future ultraviolet-optical space missions. A complete imager-cum-spectrograph assembly was constructed using off-the-shelf optical components and configured for operation in the optical band, employing a DLP9500 DMD with a 1920×1080 micromirror array. Calibration experiments established the DMD-to-detector coordinate mapping and validated the strategies for object selection and slit placement. On-sky tests in crowded stellar fields confirmed successful slit targeting, precise object alignment, and multiplexed spectral acquisition. The spectrograph achieved a peak efficiency of 32%, a spectral resolving power of $R\sim1000$ at 6000Å, a multiplexing capability of up to 46 slits (extendable to 85), and a contrast ratio of $\sim$ 6000. These results demonstrate the robustness and effectiveness of the DMD MOS system under real observational conditions and raise its TRL level for use in next-generation spectroscopic space missions.

Keywords Digital micromirror device · Multi-object spectroscopy · Astronomical instrumentation · UV astronomy · Future UV space mission · INSIST

✉ Sriram S
ssr@iiap.res.in

[1] Department of Physics and Electronics, CHRIST University, Bengaluru 560029, Karnataka, India

[2] Indian Institute of Astrophysics, Bengaluru 560034, Karnataka, India

1 Introduction

The Digital Micromirror Device, a micro-electro-mechanical system (MEMS) developed by Texas Instruments, comprises a matrix of micromirrors that can tilt between two fixed angular positions (typically ±12°, ON and OFF states), enabling dynamic control of light reflection. Originally designed for digital projection and display technologies, the DMD has more recently emerged as a promising technology in astronomical instrumentation, particularly in multi-object spectroscopy [1, 2].

In MOS systems, a configurable slit unit (CSU) is used to select multiple astronomical targets within a telescope's field of view (FoV), directing their light toward a spectrograph while rejecting unwanted background light. Traditional CSU implementations have relied on mechanical slit masks [3–7] or fiber-optic systems [8–14]. While effective, these approaches face limitations in flexibility and real-time adaptability. DMD-based CSUs overcome these limitations by allowing programmable and rapid reconfiguration of slit positions, offering significant advantages in flexibility, multiplexing efficiency, and operational simplicity.

Several ground-based DMD-based MOS systems have been developed and tested, including RITMOS [15] on the C.E.K. Mees telescope, BATMAN, developed for the Galileo telescope [16]], is currently awaiting installation, SAMOS on the SOAR telescope [17], and IRMOS for the Kitt Peak National Observatory [18]. These instruments have demonstrated the feasibility of using DMDs for optical and near-infrared spectroscopy.

On the space-based front, missions such as EUCLID, CASTOR, SUMO, and SIRMOS have explored the potential of DMDs for MOS applications in space environments [19–23]. DMDs have successfully passed critical space qualification tests, including total ionizing dose tolerance [24–26], thermal cycling, and shock and vibration tests [27, 28], underscoring their readiness for space-based deployment.

Efforts have also been made to adapt DMDs for use in the ultraviolet (UV) regime, where challenges such as surface scattering and limited window transmission arise. Solutions include replacing the standard protective window with UV-transparent alternatives and enhancing reflective coatings for improved UV efficiency [29]. These advancements further establish the DMD as a viable and flexible slit mechanism for future space-based UV spectroscopy missions.

In India, the successful deployment of AstroSat [30], the country's first multi-wavelength space observatory, and the operational success of its Ultra Violet Imaging Telescope (UVIT) [31–36], have paved the way for the INdian Spectroscopic and Imaging Space Telescope (INSIST) [37]. Proposed as a meter-class space telescope, INSIST aims to deliver high-resolution photometry in UV, u, and g bands, and includes a DMD-based MOS as one of its key instruments [38, 39].

To advance the Technology Readiness Level (TRL) of DMDs for INSIST, it is essential to validate their performance under realistic observational conditions. For this purpose, the DLP9500 DMD, featuring a 1920×1080 micromirror array with 10μm mirror pitch, was selected for evaluation. Although the final application targets UV wavelengths, initial performance testing was conducted in the optical band to assess the DMD's baseline functionality. Laboratory experiments focused on critical parameters including diffraction and reflection efficiency, contrast (light leakage),

Point Spread Function (PSF) alignment relative to micromirror gaps, and micromirror tilt repeatability.

Beyond component-level testing, a complete DMD-based imager-cum-spectrograph system was designed and built in the optics laboratory. This system enabled system-level testing of the DMD as a programmable slit unit. Key aspects investigated include:

- DMD-imager coordinate mapping,
- target selection and object masking methods,
- Light blocking efficiency,
- Throughput and spectral efficiency,
- Wavelength calibration,
- Spatial and spectral resolution dependence on slit width,
- Multiplexing capability
- Spectral contamination due to object overlap and
- Effective Field of View .

After laboratory validation, the integrated instrument was mounted on the 1.3-meter J.C. Bhattacharya Telescope (JCBT) at the Vainu Bappu Observatory. Observations were conducted in the optical band, targeting crowded star fields to assess on-sky performance under real observational conditions.

This paper presents a comprehensive report on the laboratory characterization and on-sky performance of the DMD-based Multi-Object Spectrograph. The results demonstrate the DMD's potential as a flexible and efficient slit mechanism for future UV and optical astronomical missions.

2 DLP9500 DMD

The DLP9500 DMD procured from Texas Instruments, along with the controller, is shown in Fig. 1. The DMD consists of a 2D array of 1920×1080 micromirrors, each with a size of 10μm and a pitch of 10.8μm. The micromirrors are aluminium-coated and protected by a Corning 7056 window. Each mirror in the DMD can be addressed and flipped individually or in a group to $\pm 12^\circ$ when it is powered. The flip axis passes through the diagonal of the individual mirror. The specifications of the DMD [40] are summarized in Table 1.

3 DMD MOS and imager concept

The working principle of the Digital Micromirror Device as a configurable slit mechanism for MOS is illustrated in Fig. 2. The optical telescope assembly (OTA) focuses the celestial field onto the DMD, which is mounted perpendicular to the optical axis. The imaging channel is positioned at $+24^\circ$, while the spectrograph channel is aligned at -24° relative to the optical axis. By default, all micromirrors are set to the ON state ($+12^\circ$), reflecting the entire field toward the imaging channel for broad-field obser-

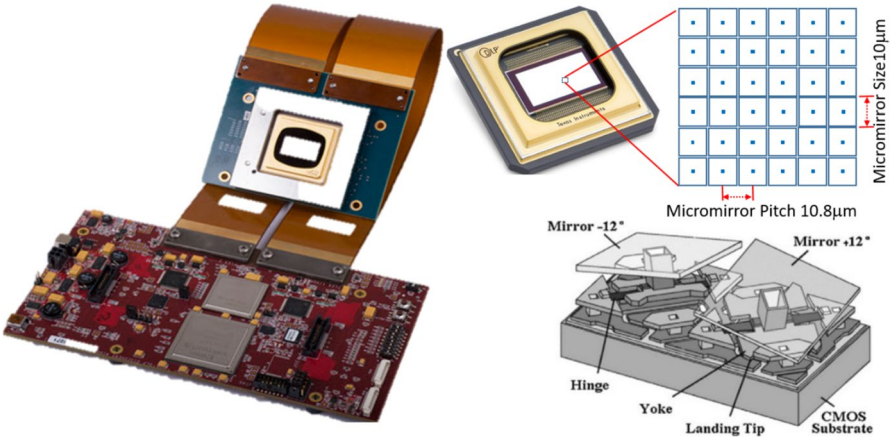

Fig. 1 The Texas Instruments DLP9500 Digital Micromirror Device used in the construction of the spectrograph and for performance evaluation in the optical band. The enlarged view illustrates the micromirror array, showing individual mirror size and pitch. The orientation of the mirrors in the ON (+12°) and OFF (-12°) states is also depicted

Table 1 DLP9500 DMD specification

Parameter	Value	Units	Remarks
Array	1920x1080	micromirrors	
Mirror width	10	μm	-
Pitch	10.8	μm	-
Mirror tilt angle	±12	degree	±1 degree
Fill factor	94	%	mirror gaps and via
Mirror Coating	Al	-	-
Mirror Reflectivity	89	%	
Array Diffraction Efficiency	87	%	-
Window	Corning7056	-	-
Window Transmission	96	%	double pass
Design Wavelength	4000-7000	Å	-

vation. For spectroscopic analysis, selected micromirrors–corresponding to target objects–are switched to the OFF state (-12°), directing their light to the spectrograph. This enables simultaneous imaging and spectroscopy, where only the spectra of designated sources are recorded while the remaining field continues to be monitored. The DMD-based MOS proposed for INSIST adopts an Offner spectrograph configuration [41], comprising two concave spherical mirrors (OM1, OM2) and a convex ruled blazed grating for dispersion. The imaging arm utilizes the same Offner mirrors (OM1, OM2) along with a convex mirror (M) for wide-field detection.

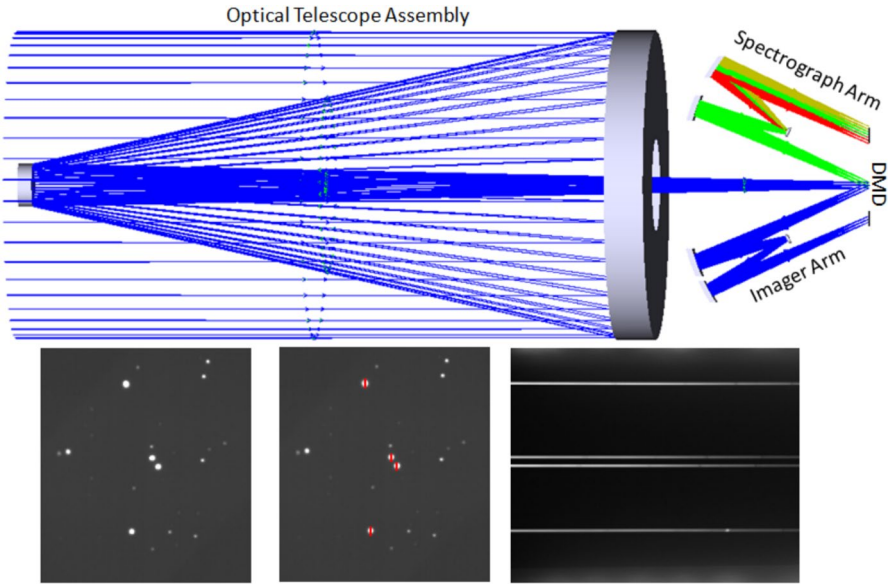

Fig. 2 Concept of the Digital Micromirror Device application in an astronomical telescope as a configurable slit mechanism for Multi-Object Spectroscopy. **Top:** The Optical Telescope Assembly focuses celestial objects onto the DMD, which directs light to the imager and spectrograph positioned on either side of the optical axis at (+24°) and (-24°) respectively. **Bottom Left:** The celestial field as captured by the telescope. **Bottom Middle:** Slits positioned over objects of interest for obtaining spectra. **Bottom Right:** Spectral image of the objects selected by the DMD slits

The target selection and spectral acquisition procedure follows these steps:

- **Field Imaging:** Set all DMD micromirrors to ON (+12°) to capture the full field in the imaging channel.
- **Target Identification:** Select astronomical targets and record their detector coordinates (X_D, Y_D).
- **Coordinate Mapping:** Convert detector coordinates to DMD mirror positions (X_{DMD}, Y_{DMD}) using pre-calibrated alignment data (Detector-DMD mapping data).
- **Slit Definition:** Assign slit dimensions (width/height) based on scientific requirements (e.g., source brightness, spectral resolution).
- **Mirror Selection:** Generate a configuration file specifying the micromirrors to be switched OFF (-12°) around each target's (X_{DMD}, Y_{DMD}) position.
- **Slit Configuration:** Upload the configuration FILE to the DMD controller, creating virtual slits under the targets.
- **Spectral Acquisition:** Begin spectrograph exposure to record target spectra.
- **Field Tracking:** The imager continues monitoring the field during spectroscopy, enabling real-time telescope tracking to maintain slit-target alignment.

The bottom row of Fig. 2 illustrates the process of object selection in the DMD-based spectrograph system: the celestial field as it falls on the DMD, the placement of

virtual slits over the target objects, and the resulting spectral images of the selected objects recorded by the spectrograph.

4 DMD based MOS and imager: Optical design

The optical layout of the imager and spectrograph, as described in the previous section, represents the proposed design for the upcoming INdian Spectroscopic and Imaging Space Telescope (INSIST) mission. This system is fully optimized for ultraviolet (UV) wavelengths in the range of 1500Å–3000Å and is based on a simplified Offner configuration, where a convex grating serves as the dispersive element. The primary advantage of this all-reflective Offner-type design lies in its inherent freedom from chromatic aberration, diffraction-limited image quality, and a naturally flat focal plane.

However, due to the unavailability of a convex grating for current implementation, a laboratory version of the spectrograph and imager was designed using achromatic doublets and a transmission grating. This setup was customized to match the specifications of the 1.3-meter JCB Telescope at Vainu Bappu Observatory.

The 1.3-meter aperture JCB telescope delivers an f/8 beam at its Cassegrain port with the plate scale of 50μm/$''$. The DMD DLP9500 at the telescope focal plane covers the FoV of 6.8 x3.8 with 0.2$''$/micromirror. The design parameters of the spectrograph, imager, and the JCB Telescope are summarized in Table 2. The optical configuration, created using ZEMAX/Optics Studio, is illustrated in Fig. 3. The system is divided into three functional arms:

- the spectrograph arm
- the imager arm and
- the calibration arm.

The imager arm, aligned at +24° with respect to the optical axis of the telescope, consists of collimator and camera optics with an effective focal length (EFL) of 150 mm. Due to the mechanical constraint imposed by the limited distance between the mounting and focal planes, a fold mirror is incorporated to redirect the beam to the detector. When the DMD mirrors are set to +12°(ON state), the incoming light from the sky is reflected directly into the imager, enabling imaging. The optical design is optimized for the field covered by DMD in 1:1 imaging. The detector presently available (CMOS, 2560x2160 pixels, 6.5μm pixel) covers a limited FoV ($\sim$4 x3) with 0.13”/pixel coverage.

The spectrograph arm, aligned at -24°, also uses a 150 mm EFL collimator-camera pair, operating in a 1:1 imaging mode. A 600 lines/mm transmission grating, blazed at 8.3° for 5000Å, is used to disperse the incoming light. A fold mirror is added to accommodate mechanical layout constraints. The grating operates in first order, covering the 5000Å–7500Å wavelength range for the central DMD field. When the DMD mirrors are set to -12° (OFF state), light from selected objects is directed into the spectrograph. The design is optimized for the spectral resolution R$\sim$2000 at wavelength 5000Å with the slit formed by 2x2 mirrors. The FWHM of the spectral

Table 2 Primary optical specification of DMD-based Slit-MOS/Imager designed for 1.3meter JCB Telescope

Description	Specification	Remarks
JCB Telescope Parameters		
Aperture	1.3m	0.3 obscuration
Working F/#	8	Fold cassegrain port
Corrector	3 Elements	BK7 glass
Image Quality	Seeing limited	Seeing < 1.5″
Feld of View	45	Unvigenetted
Plate scale	19.8″/mm	∼50μm/″
DMD Slit-MOS design parameters		
DMD Array	1920×1080 micromirrors	20.7mm×11.6mm
Mirror size	10 μm ×10 μm	0.2″x0.2″
DMD Field coverage	6.8 x3.8	45 degree rotated on sky
Camera-Collimator f/#	8	telescope f/# Matching and 1:1 imaging
Wavelength Coverage	5000-7500Å	for the object at DMD center
Spectral Resolution	2.5Å@ 5000Å[R∼2000]	slit width set by 2x2mirror
Spectral Resolution	6.0Å@ 6000Å[R∼1000]	slit width set by 5x5mirror
Spatial Resolution	3.6″	for slit length 3″
Multiplexing	>50	for slit length 3″
Detector	2560x2160 CMOS array	16.6mmx14.0mm, 6.5μm pixel
Detector field coverage	4 x3	limited by detector size
Imager design parameters		
Camera-Collimator f/#	8	telescope f/# Matching and 1:1 imaging
Detector	2160x2560 CMOS array	16.6mmx14.0mm, 6.5μm pixel
Detector field coverage	4 x3	limited by detector size
Pixel scale	0.13″	-

image on the detector covers 3pixels with each pixel subtending 0.13″. The extend of the spectra of full wavelength coverage occupies ∼3000 pixels on the detector. The presently available detector will be able to cover 90% of wavelength coverage for the object at the center of the DMD. Also, the detector limits the over all FoV of the spectrograph. In future, a large format detector is proposed to be used in the spectrograph to cover the maximum FoV and the full wavelength coverage.

The calibration arm provides wavelength and flat-field calibration using Neon and Xenon light sources, respectively. Light from each source is coupled into optical fibers and delivered to the DMD through dedicated collimation optics. The calibration unit's layout is shown in Fig. 4, and the complete optical layout, including the

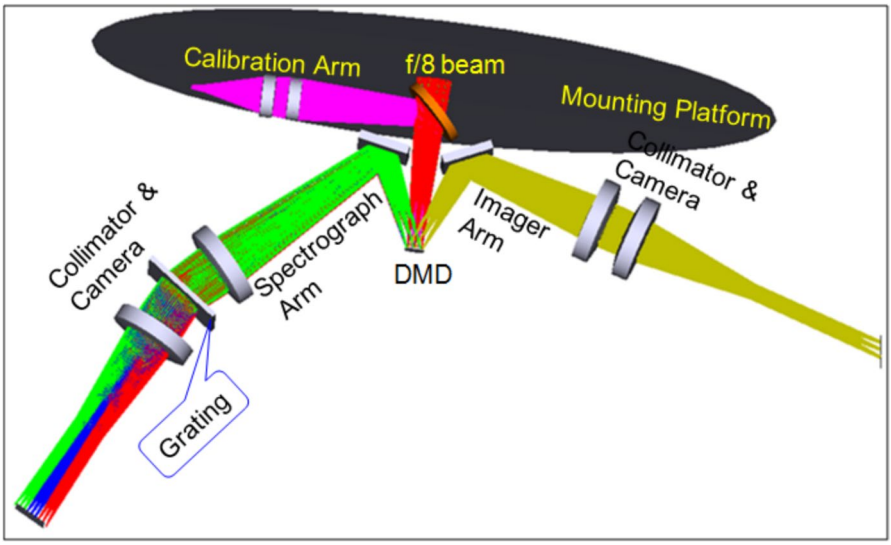

Fig. 3 DMD-based multi-object spectrograph cum imager optical layout. The typical design of the spectrograph and imager follows the Offner configuration with all reflective optical components

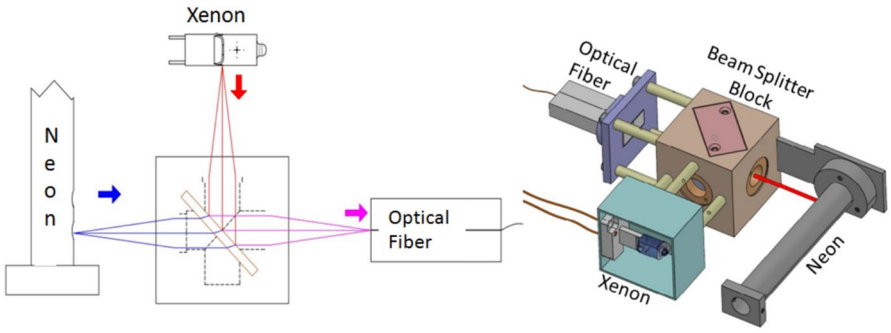

Fig. 4 DMD Slit-MOS Calibration Unit: **Left:** Optical layout of Neon source for wavelength calibration and Xenon for flat fielding coupled into the optical fiber is depicted. The output end of the fiber is taken in the calibration arm, and the DMD through set of optics in the calibration arm. **Right:** illustrates the mechanical model of the calibration unit

spectrograph, imager, and calibration unit integrated with the JCB Telescope, is presented in Fig. 5.

5 MOS and imager integration and testing

5.1 Imager integration and testing

The mechanical structure for the spectrograph/imager assembly was designed using the SolidWorks CAD software and is shown in Fig. 6. The entire assembly is con-

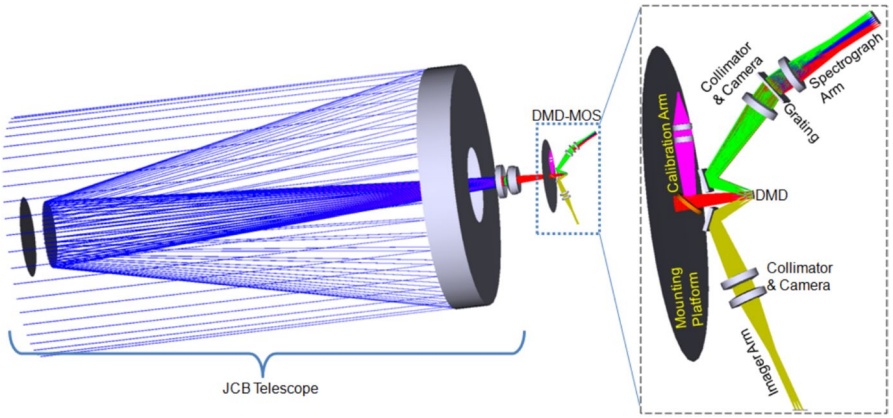

Fig. 5 DMD-based Slit-MOS mounted on JCB Telescope. MOS with three arms: Spectrograph Arm, Imager Arm and Calibration Arm are illustrated

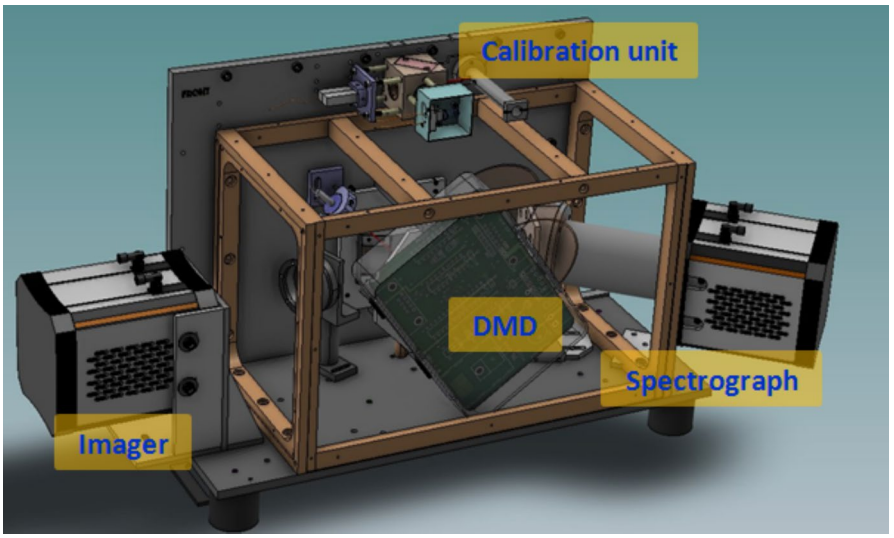

Fig. 6 The DMD MOS/Imager mechanical structure designed in SolidWorks is shown. The calibration unit is located at the top of the structure

structed from aluminium, chosen for its mechanical and thermal stability. The calibration unit, which houses both the wavelength calibration (Neon) and flat-fielding (Xenon) lamps, is positioned at the top of the structure for ease of integration and accessibility.

All optical components of the imager, spectrograph, and calibration arms were integrated into the mechanical assembly, as illustrated in Fig. 7. Initial alignment of the system was performed in the laboratory using a series of laser beams to ensure proper alignment of all optical elements with respect to the DMD. After

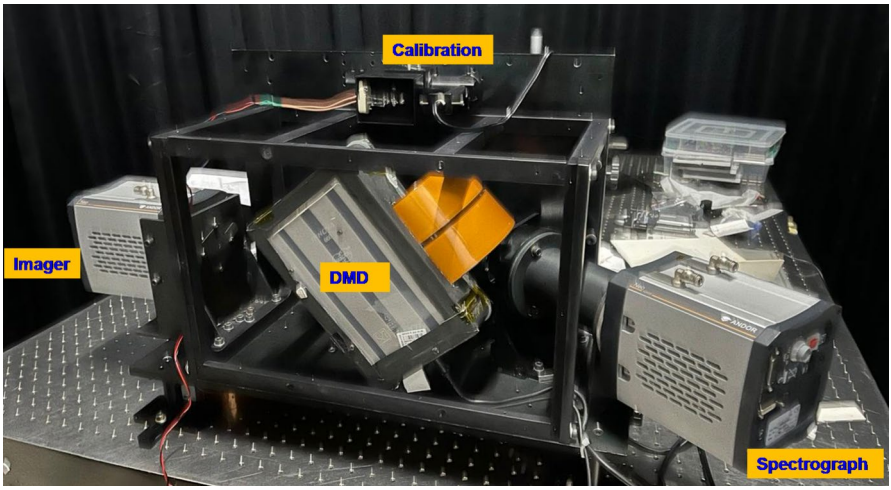

Fig. 7 The DMD-based Slit-MOS integrated and aligned within its mechanical structure is shown. The system features two detectors: one dedicated to the imager and the other to the spectrograph. The calibration unit, which provides input to the DMD, is positioned at the top of the setup

the alignments, the detector (Andor NEO 5.5 CMOS) was mounted at the focal plane of the imager.

To verify alignment and optical performance, a 10×10 grid of slits was generated on the DMD. Each slit was composed of 5x15 micromirrors, corresponding to an on-sky coverage of $\sim1''$x$3''$, with a spacing of 100 micromirrors between adjacent slits. These slits were programmed with the DMD in the +12° (ON) state and illuminated using a Xenon flat-field source. The resulting image of the slit grid was captured on the imager and used to align the detector and optimize the focus in the imager arm.

The captured image of the slit grid and the corresponding Line Spread Function (LSF) of a single slit are shown in Fig. 8. The LSF exhibits a Full Width at Half Maximum (FWHM) of approximately 9 pixels, with each detector pixel corresponding to $0.13''$. The variation in LSF across the detector is $\sim$1 to 2 pixels, and the variation is mainly attributed to the limitation of the achromatic doublet lenses used as collimator and camera.

5.2 DMD detector coordinate mapping

The selection of target objects for spectroscopy from the telescope field is performed using the imager, which captures the field projected onto the DMD plane. The light from the telescope is directed onto the DMD, and the DMD's ON-state mirrors (+12°) reflect the field to the imager detector, where a full-field image is recorded. From this image, the detector coordinates (X_D,Y_D) of the desired objects are identified.

To accurately direct light from a selected object to the spectrograph, it is essential to determine the corresponding DMD mirror coordinates (X_{DMD},Y_{DMD}). This requires a detector-to-DMD coordinate mapping, which is established through calibration by forming a known grid of slits on the DMD and recording their corresponding centroids on the detector.

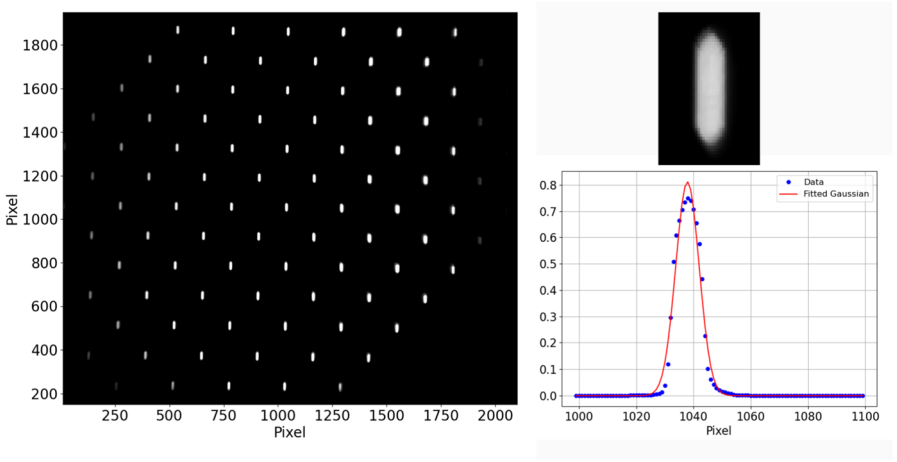

Fig. 8 The image of the slit grid, each formed by a 5x15 micromirror array, captured on the detector in the Imager Arm is shown on the left. This grid pattern is utilized to align and fix the Imager Arm detector focus. The insert in the right plot shows the enlarged view of a single slit image. The LSF of the single-slit image is shown on the right and its FWHM measured as 9 pixels ($\sim 1.1''$)

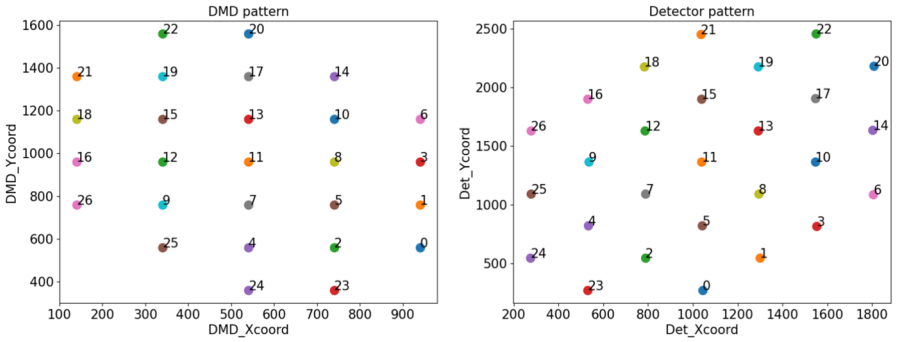

Fig. 9 DMD-Detector Mapping. **Left:** Grind of slit centers formed 5x5 DMD mirrors. **Right:** Centroid coordinates of the slit images formed on the detector. The numbers in the plots indicate the slit number on the DMD and the corresponding slit image on the detector used for mapping

The calibration grid is generated using 5×5 micromirror arrays to form individual slits at known DMD positions. The resulting images are used to derive the mapping between DMD and detector coordinates. A set of DMD slit coordinates and their associated image centroids on the detector is presented in Fig. 9.

To determine the DMD slit coordinates corresponding to a given detector coordinate, an interpolation is performed using the calibration data. The residual deviations in both the X and Y axes–i.e., the difference between the expected and actual slit positions on the DMD–are calculated and plotted in Fig. 10. These residuals show a Maximum deviation of approximately 2 micromirrors in both axes, with the largest discrepancies occurring at the top and bottom edges of the DMD array.

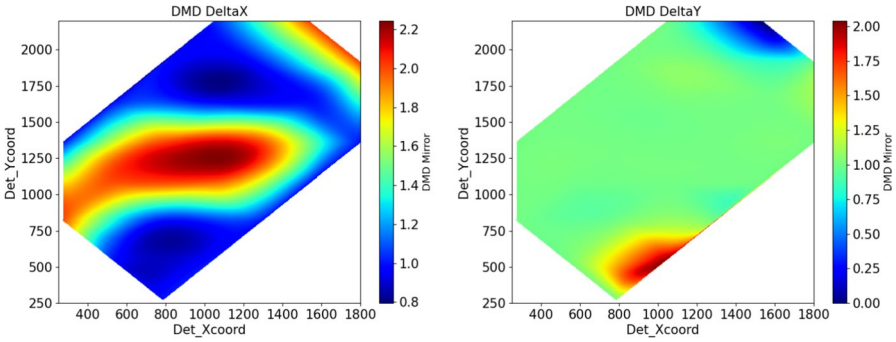

Fig. 10 DMD-Detector Residual Distortion. **Left:** Deviation of DMD mirror positions (X-coordinates) corresponding to the image coordinates of objects in the imaging field. **Right:** Same as the left but for Y coordinates. The Maximum deviation of approximately 2 micromirrors is observed at the top and bottom edges of the DMD

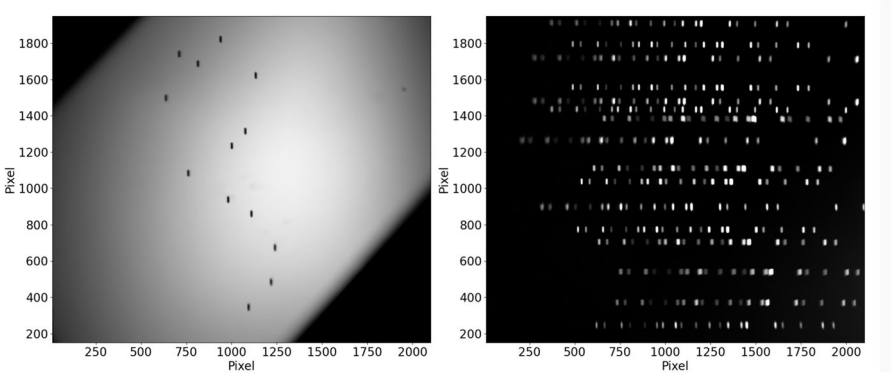

Fig. 11 **Left:** The set of slits used for the integration, testing and alignment of the spectrograph is shown. **Right:** The spectra of the neon source registered on the detector for the selected slits are shown

These residuals are accounted for during the object selection process to ensure accurate placement of virtual slits over the selected targets on the DMD, thereby improving the spectral acquisition precision and minimizing slit misalignment.

5.3 Spectrograph integration and testing

The optical components–collimator, diffraction grating, and camera lenses–are integrated into the mechanical structure and aligned using a He-Ne laser. The detector (Andor NEO 5.5 CMOS) is mounted at the focal plane of the spectrograph. A set of slits, formed with a 5×15 micromirror array as shown in Fig. 11 (Left), is illuminated using a neon source. The dispersed spectral images are recorded on the detector, and the detector position is aligned for focus. The recorded spectral images on the detector are shown in Fig. 11 (Right). The spectra of the neon source for the slit at the center of the field are shown at the left of Fig. 12, and the PSF of the spectral line in pixel coordinates is shown at the right.

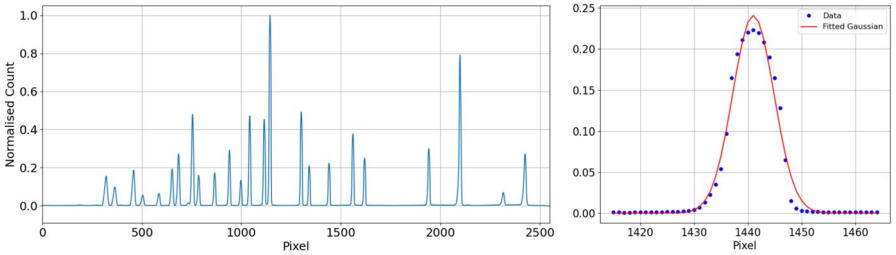

Fig. 12 **Left:** The spectra of the neon source for the slit at the center of the field are plotted. **Right:** The PSF of the single emission line is shown in pixel coordinates. The FWHM of the PSF closely matches the slit width (∼9.2pixels)

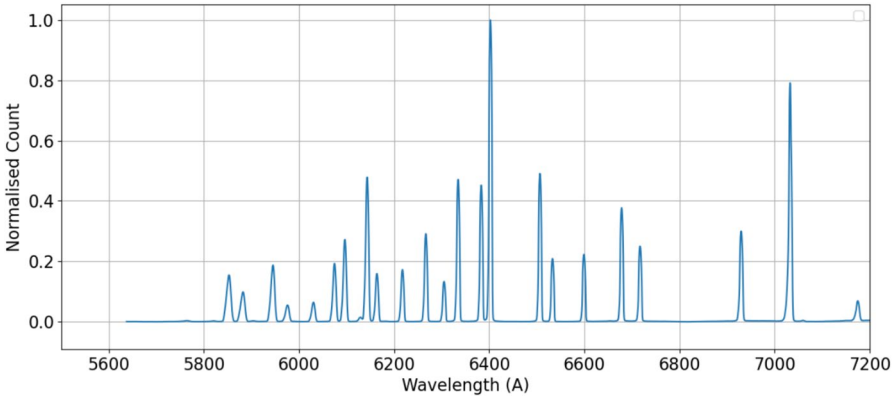

Fig. 13 Wavelength-calibrated spectra of the neon source for the slit at the center of the field of view

5.4 Spectrograph analysis

The spectra recorded from the Neon calibration source, initially in pixel coordinates, were converted into wavelength coordinates using a wavelength calibration procedure. The calibrated spectrum corresponding to the central slit in the field is shown in Fig. 13. The spectral coverage for this slit ranges from 5250Å to 7200Å, constrained by the size of the detector. The dispersion across the spectral range is linear, with a measured value of approximately 0.66Å/pixel. The point spread function (PSF) of the spectral lines spans approximately 9.2 pixels, yielding a spectral resolving power of R∼1000 at 6000Å. For objects aligned along the spatial (vertical) direction of the detector, both the linear dispersion and spectral resolution remain uniform across the field. However, objects located toward the edges of the field in the dispersion (horizontal) direction exhibit noticeable PSF broadening (∼10-12 pixels), leading to a decline in spectral resolution. This degradation is primarily attributed to the inability of the current collimator and camera optics to fully compensate for field curvature at large off-axis angles. The region delivering consistent image quality and spectral resolution–referred to as the useful field of view–is approximately 4 x3 , centered on the DMD.

To evaluate system throughput, the spectrograph efficiency was calibrated at selected wavelengths between 5500Å and 7500Å using a monochromatic source and a NIST-calibrated detector, as shown in Fig. 14. The spectrograph achieved a Maximum efficiency of 32% at 5500Å. The observed efficiency decline at longer wavelengths is primarily due to the reduced performance of the diffraction grating and the quantum efficiency of the detector.

5.5 DMD MOS multiplexing

The multiplexing capability of the MOS was tested for the JCB Telescope using two slit configurations. In the first test, 5x15 mirror slits ($1'' \times 3''$) were arranged along the spatial direction on the DMD, with a gap of 3 mirrors between slits to prevent contamination. These slits were set to the OFF state (-12°) and illuminated using a neon source. The resulting slit images on the imager and corresponding spectra on the spectrograph are shown in Fig. 15. This configuration demonstrated a Maximum multiplexing capacity of 46 slits without contamination. In the second test, 5×10 mirror slits ($1'' \times 2''$) were used, Maintaining a 3-mirror gap between slits. This configuration increased the multiplexing capability to 85 with no spectral contamination along the spatial direction.

5.6 Contrast

The contrast measurement adopted in the laboratory closely follows the established methods [42, 43]. An f/8 beam was generated from the neon emission lamp using optical fiber, a pinhole, and a set of reimaging optics as shown in Fig. 16. DMD was illuminated with the f/8 beam yielding tight PSF ($\sim 0.5''$ FWHM). All the DMD mirrors were set to the ON state and directed the light towards the imager arm. The

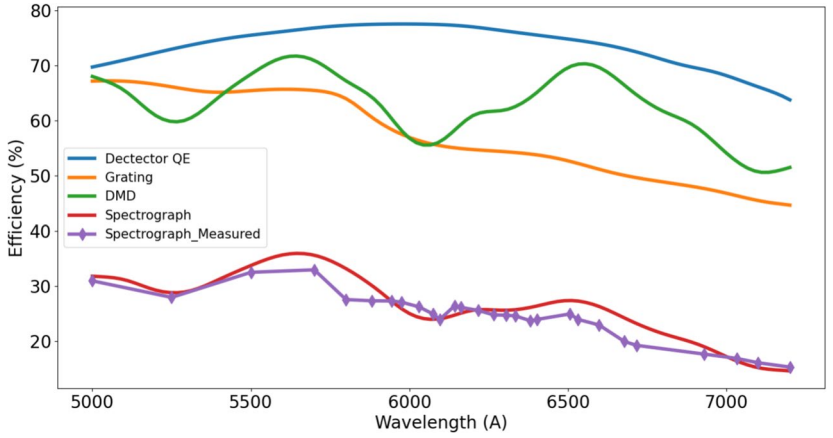

Fig. 14 The spectrograph efficiency: The measured spectrograph efficiency at discrete monochromatic wavelengths was obtained using a NIST-calibrated detector in the laboratory. The efficiency plot shows a peak value of 32% at 5550Å, with a decline at longer wavelengths. This reduction in efficiency is primarily attributed to the lower diffraction grating efficiency and the detector's quantum efficiency (QE)

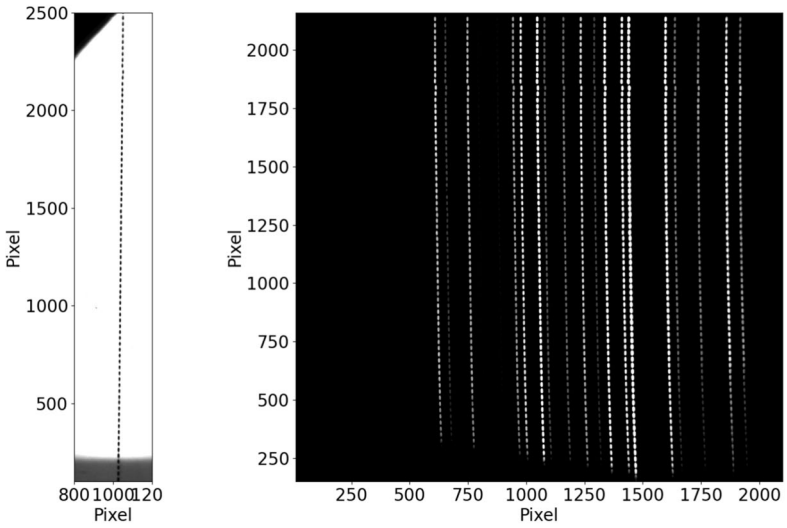

Fig. 15 DMD MOS Multiplexing. **Left:** Slits formed by 5×15 mirrors stacked along the spatial direction on the DMD, recorded on the imager. **Right:** Spectra of the neon source through the slits, registered on the spectrograph. The achieved multiplexing capacity is 46

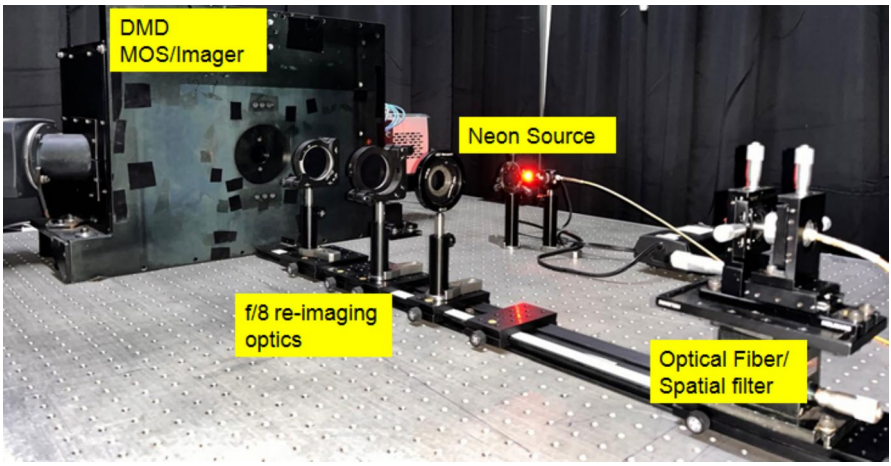

Fig. 16 DMD contrast measurement test setup: The light from the source (Neon or Xenon lamp) is delivered via an optical fiber into a spatial filter (pinhole). The emerging beam is then reimaged to form an f/8 beam, which is focused onto the DMD to produce a tight PSF for the DMD contrast evaluation

total signal falls on the spectrograph arm detector over the exposure time T_{ON} was recorded, and the background-subtracted count ($Signal_{\mathrm{ON},\lambda}$) under each wavelength was extracted. Then all the mirrors were turned to the OFF state away from the imager, the flux falls on the spectrograph arm detector over the exposure T_{OFF} was again

registered, and the background-subtracted count ($Signal_{\mathrm{OFF},\lambda}$) were extracted. The spectral images (a portion) registered on the spectrograph detector in all mirrors ON and OFF states with the exposure adjustment are depicted in Fig. 17 with the color bar. The intensity scale of the images differ by a factor of 1000.

Similar to the spectrograph channel, the contrast measurements in the imager arm were also conducted over the 5000Å to 7500Å range. Monochromatic light from a Xenon lamp was selected by a spectrometer, then coupled into an optical fiber and reimaging optics setup to generate f/8 beam. This f/8 beam was focused onto the DMD for contrast testing. The rest of the procedure follows the spectrograph arm contrast measurement. The following expression is used for deriving the contrast of the DMD at a given wavelength.

$$\mathrm{Contrast}(\lambda) = \frac{T_{\mathrm{ON}}}{T_{\mathrm{OFF}}} \times \frac{\mathrm{Signal}_{\mathrm{ON},\lambda}}{\mathrm{Signal}_{\mathrm{OFF},\lambda}}$$

The contrast of DMD measured in spectrograph channel with neon source and in the imager channel with the xenon lamp and spectrometer over the wavelength 5000Å-7500Å are plotted in Fig. 18. The red squares represent the contrast of the DMD measured in the spectrograph arm, whereas the blue dots in the imager arm. The resulting contrast values in the imager and spectrograph arms are closely match and confirming consistent performance across both channels. The resulting contrast values also show good agreement with those are reported in [42, 43].

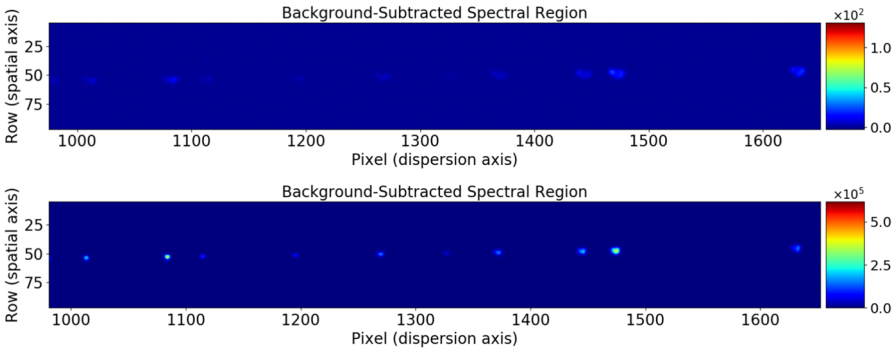

Fig. 17 Example of a portion of background subtracted spectra taken by spectrograph with a Neon source. The top plot shows a spectrum taken with all of the micromirrors in the "ON" state, facing the imaging channel. The bottom plot shows a readout of the same section when all of the micromirrors are in the "OFF" state, facing towards the spectroscopic channel. The intensity scale of the plots differ by a factor of 1000

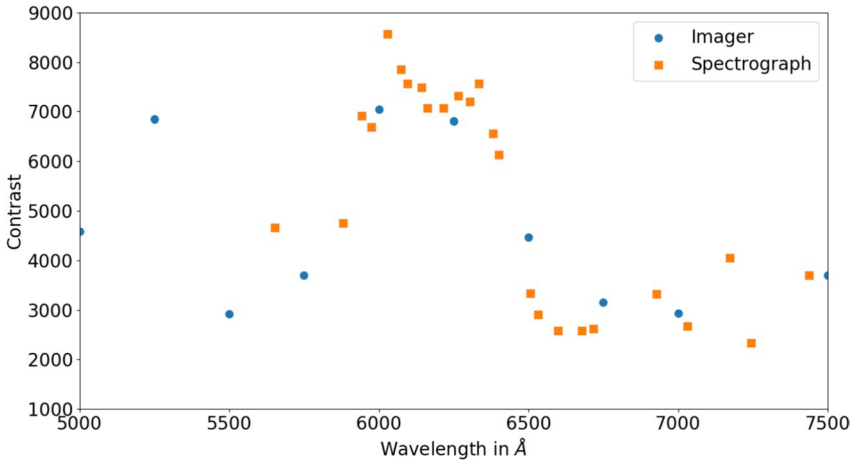

Fig. 18 The plot shows the contrast ratio of DMD measured in spectrograph and imager arm over the wavelength region 5000Å-7500Å. Red squares represent the contrast values at the respective wavelengths resulted in the spectrograph arm and the blue dots are for the image arm

6 DMD MOS at JCB telescope

6.1 Observations

The integrated DMD-based MOS was mounted on the side port of the JCB telescope at VBO (Fig. 19) and the observations were carried out. The primary objectives were to verify the DMD's ability to:

- Select objects from the imaging field.
- Accurately place slits over the selected objects.
- Demonstrate its multiplexing capabilities effectively.

The observation sequence for the DMD-MOS was as follows:

- Point the telescope towards the desired field.
- Image the field using the imager, with all DMD mirrors set to the "ON" state (+12°).
- Identify the object coordinates from the imaged field for spectral acquisition.
- Feed the object coordinates in the DMD-Detector coordinate mapping program to get the corresponding DMD coordinate file.
- Input the DMD coordinates file into the slit selection program and also set the slit widths and heights.
- Execute the DMD interface program to place slits over the selected objects.
- Confirm the slit placement on the targeted objects using the imager.
- Begin exposure on the spectrograph detector to record the spectra.
- Use the imager to guide and track objects on the slits during exposure.

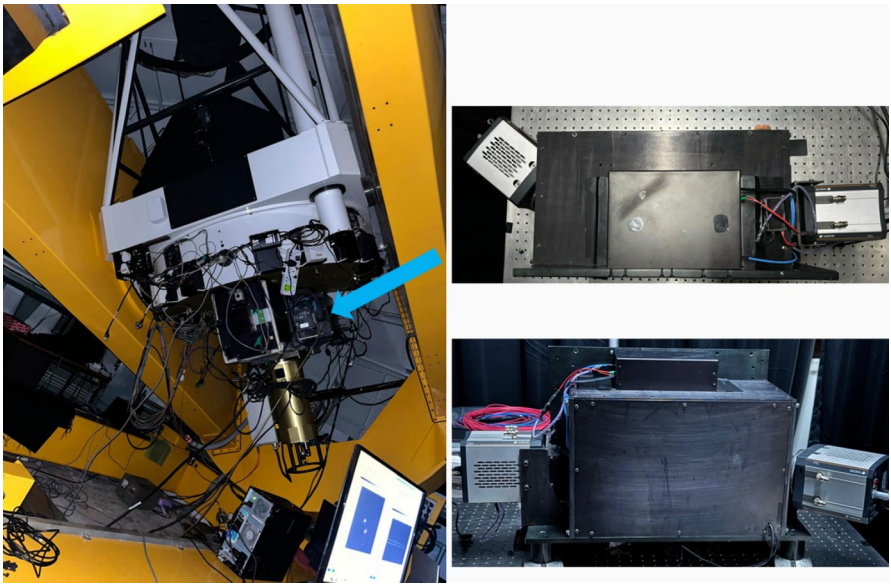

Fig. 19 DMD MOS on JCBT is shown. **Left:** DMD-based Multi-Object Spectrograph (MOS) mounted on the side port of the JCB telescope (indicated by arrow), fed by an f/8 beam via a fold mirror (not visible in the image). **Top Right:** Top view of the DMD MOS, showing two detectors–one for imaging and the other for the spectrograph. **Bottom Right:** Front view of the MOS

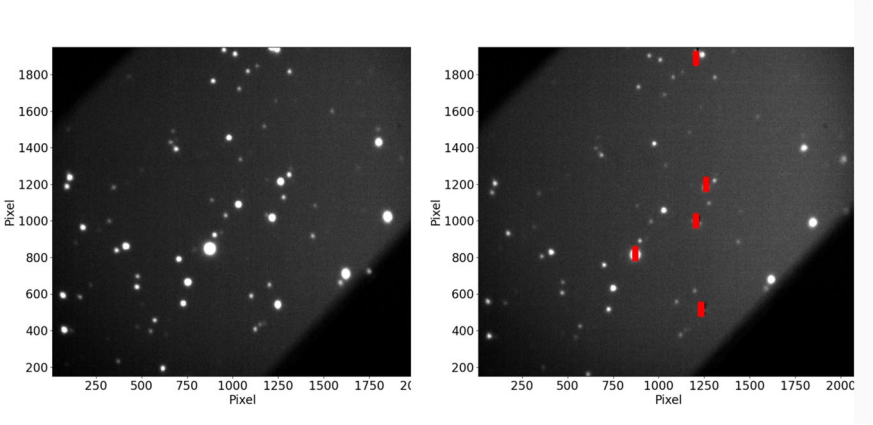

Fig. 20 The open cluster NGC 2099 (M37, RA = 5h 52.4m, Dec = +32° 33') imaged, is shown in the left panel. The slits formed by a 5x15 mirror of DMD (1″ x 3″) and placed over the objects (five objects) are shown in the right panel

The open cluster NGC 2099 (M37) (RA = 5h 52.4m, Dec = +32° 33') was selected for testing DMD-based MOS performance. The field was imaged using the DMD imager, as shown in the left panel of Fig. 20. From the imaged field, the detector coordinates of objects targeted for spectral analysis were determined. A slit size of 5x15

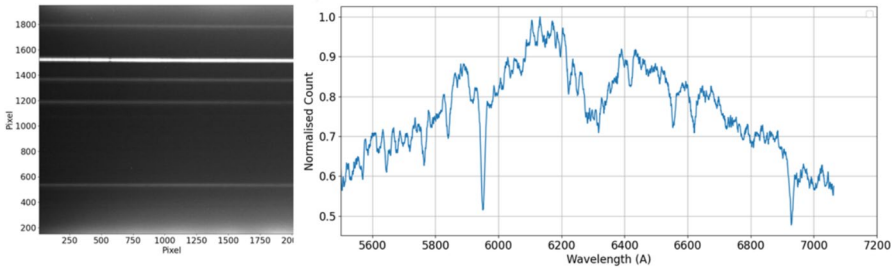

Fig. 21 DMD-MOS spectra of NGC2099. **Left:** Spectral images of the objects selected by 5x15 mirror slits from the NGC2099 open cluster. **Right:** Extracted spectra of the bright spectral image

Table 3 DMD MOS observational results summary

Description	Design Value	Achieved	Remarks
Wavelength Coverage	5000Å-7500Å	5200Å-7200Å	Limited by detector
Field of View	6.8 x3.8	$\sim$ 4 x3	DMD is 45° rotated
Slit	0.4″x3″	1″x3″	Limited by seeing disc
FWHM	9 pixels	9.2pixels	10 pixels at the edge
Spectral Resolution	1000 at 6000Å	$\sim$988 at 6000Å	1″ slit width
Spectral Resolution	2000 at 6000Å	$\sim$1980 at 6000Å	0.4″ slit width
Spatiall Resolution	3″	3.6″	Limited by 1″ x3″ slit
Multiplexing	50	46	Limited by 1″x 3″ slit
Slit placement accuracy	<0.1″	0.1″	-

mirrors ($1'' \times 3''$) was chosen and applied to the selected objects. The slit placement accuracy was observed to be $\sim$1 pixel on the detector (equivalent to $0.13''$).

The right panel of Fig. 20 shows the placement of slits over five objects in the field. The recorded spectra of the five selected objects and the extracted spectrum of the brightest object are presented in Fig. 21.

6.2 Observation results

The results from observations conducted at JCBT using the DMD-based Multi-Object Spectrograph are summarized in Table 3. Pixel-to-wavelength conversion

was performed using a neon spectral calibration source in IRAF and Python Astropy packages [44–48]. The observed multiplexing capability was constrained by both the number of objects in the field of view and the detector size.

A maximum spectral resolution of ∼2000 was achieved for bright objects using a 0.4″ slit width, aligning with the design expectations. Additionally, the slit placement accuracy was achieved as anticipated, confirming the system's precision in object selection and spectral acquisition.

7 Summary

The Multi-Object Spectrograph with configurable slits using a Digital Micromirror Device was designed in ZEMAX [49] using off-the-shelf optical components and detectors. Comprehensive laboratory testing of the DMD demonstrated excellent performance. The mechanical structure for the MOS, including the spectrograph, imager, and calibration units, was designed and integrated in-house using SolidWorks and ACAD packages [50, 51]. Laboratory tests revealed a spectrograph efficiency peaking at 32% within the 5500Å–7500Å range, a linear dispersion of 0.66Å/pixel, and a resolution of R∼1000 at 6000Å. The MOS was installed on the JCB telescope at the Vainu Bappu Observatory and tested with the NGC 2099 open cluster. Field performance showed slit placement accuracy within 0.13″ and also matched the laboratory-calibrated resolution. The MOS demonstrated a multiplexing capability of up to 46 slits with 5×15 mirrors, and the multiplexing increases to 86 for 5×10 mirror slits. MOS also achieves contrast in the range ∼ 1:3000 to 1:8000 over the wavelength region 5000Å-7500Å. The integration of the MOS with the DMD-based configurable slits represents a significant achievement. The performance results, both in the laboratory and in the field, confirm the reliability and efficiency of the system. The system demonstrates high precision in slit placement, excellent contrast, and effective resolution for spectroscopy.

8 Future work

The current on-sky performance of the DMD-based spectrograph and imager has been limited, primarily due to the use of simple achromatic doublets as collimator and camera optics. To achieve improved imaging and spectroscopic performance, the optical system must be upgraded with multi-element collimators and camera lenses, designed specifically for wide-field, low-aberration performance.

In addition, replacing the existing transmission grating with a blazed reflection grating could significantly enhance spectral throughput. The present 1:1 reimaging system leads to field vignetting, limiting the ability to fully utilize the DMD area. Introducing a reimaging camera with a demagnification factor would allow accommodation of the entire DMD field on the detector, thereby expanding the effective field of view.

The spectrograph design also requires optimization for the wavelength range of 4000Å to 7500Å, ensuring full spectral coverage within the available detector space. Improving the system's overall efficiency–currently measured at 32% peak throughput–is a critical area for enhancement. This can be addressed through optical redesign, improved coatings, and higher-efficiency gratings.

Furthermore, to improve operational efficiency during observations, particularly over larger fields of view, the development of automated slit selection algorithms is essential. This would significantly reduce manual intervention, enabling real-time target acquisition and enhanced multiplexing capability.

Acknowledgements We sincerely thank the entire optics team–Chetan, Nataraj, Totan Chand, and Amirul–at the Indian Institute of Astrophysics for their invaluable support during the laboratory experiments. We also extend our gratitude to Vishnu Unni, Anwesha Hoodati, and Akhil Jaini for their contributions during the early stages of instrumentation development. Special thanks are due to the observational and mechanical teams at the observatory for their assistance during the on-sky observations. We are grateful to the observatory scientist in charge and the telescope in-charge for facilitating telescope time and supporting the object selection process essential for testing the spectrograph.

Author Contributions A. The first author Sriram Sripadmanaban contributed to the concept and the experiments, drafted the manuscript. B. The second author Vineeth Valsan contributed to the concept and the experiments, drafted the manuscript. C. The third author Remya B.S contributed to the experiments. D. The fourth author Annapurni Subramanium contributed to the concept, observation, and reviewed the manuscript. E. The fifth author Maheswar Gopinathan contributed to the concept, observation, and reviewed the manuscript.

Funding This research was made possible through financial support from the Indian Institute of Astrophysics (IIA) under the Department of Science and Technology (DST) in India.

Data Availability Data can be available on request.

Declarations

Competing Interests The authors declare no competing interests.

References

1. Ma, J.: Advanced mems-based technologies and displays. Displays **37**, 2–10 (2015). https://doi.org/10.1016/j.displa.2014.10.003. Advanced MEMS technologies and Displays
2. Robberto, M., Cimatti, A., Jacobsen, A., Zamkotsian, F., Zerbi, F.M.: Applications of DMDs for astrophysical research. In: Hornbeck, L.J., Douglass, M.R. (eds.) Emerging Digital Micromirror Device Based Systems and Applications. Society of Photo-Optical Instrumentation Engineers (SPIE) Conference Series, vol. 7210, p. 72100 (2009). https://doi.org/10.1117/12.809542
3. Le Fèvre, O., Saisse, M., Mancini, D., Brau-Nogue, S., Caputi, O., Castinel, L., D'Odorico, S., Garilli, B., Kissler-Patig, M., Lucuix, C., Mancini, G., Pauget, A., Sciarretta, G., Scodeggio, M., Tresse, L., Vettolani, G.: Commissioning and performances of the VLT-VIMOS instrument. In: Iye, M., Moorwood, A.F.M. (eds.) Instrument Design and Performance for Optical/Infrared Ground-based Telescopes. Society of Photo-Optical Instrumentation Engineers (SPIE) Conference Series, vol. 4841, pp. 1670–1681 (2003). https://doi.org/10.1117/12.460959

4. Faber, S.M., Phillips, A.C., Kibrick, R.I., Alcott, B., Allen, S.L., Burrous, J., Cantrall, T., Clarke, D., Coil, A.L., Cowley, D.J., Davis, M., Deich, W.T.S., Dietsch, K., Gilmore, D.K., Harper, C.A., Hilyard, D.F., Lewis, J.P., McVeigh, M., Newman, J., Osborne, J., Schiavon, R., Stover, R.J., Tucker, D., Wallace, V., Wei, M., Wirth, G., Wright, C.A.: The DEIMOS spectrograph for the Keck II Telescope: integration and testing. In: Iye, M., Moorwood, A.F.M. (eds.) Instrument Design and Performance for Optical/Infrared Ground-based Telescopes. Society of Photo-Optical Instrumentation Engineers (SPIE) Conference Series, vol. 4841, pp. 1657–1669 (2003). https://doi.org/10.1117/12.460346
5. Kashikawa, N., Aoki, K., Asai, R., Ebizuka, N., Inata, M., Iye, M., Kawabata, K.S., Kosugi, G., Ohyama, Y., Okita, K., Ozawa, T., Saito, Y., Sasaki, T., Sekiguchi, K., Shimizu, Y., Taguchi, H., Takata, T., Yadoumaru, Y., Yoshida, M.: FOCAS: The faint object camera and spectrograph for the Subaru telescope. PASJ **54**(6), 819–832 (2002). https://doi.org/10.1093/pasj/54.6.819
6. Ichikawa, T., Suzuki, R., Tokoku, C., Uchimoto, Y.K., Konishi, M., Yoshikawa, T., Yamada, T., Tanaka, I., Omata, K., Nishimura, T.: MOIRCS: multi-object infrared camera and spectrograph for SUBARU. In: McLean, I.S., Iye, M. (eds.) Ground-based and Airborne Instrumentation for Astronomy. Society of Photo-Optical Instrumentation Engineers (SPIE) Conference Series, vol. 6269, p. 626916 (2006). https://doi.org/10.1117/12.670078
7. Allen, D.A., Barton, J.R., Burton, M.G., Davies, H., Farrell, T., Gillingham, P., Lankshear, A., Lindner, P., Mayfield, D., Meadows, V., Schafer, G., Shortridge, K., Spyromilio, J., Straede, J., Waller, L., Whittard, D.: IRIS: An infrared imager and spectrometer for the Anglo-Australian telescope. PASA **10**(4), 298 (1993). https://doi.org/10.1017/S1323358000025911
8. Smee, S.A., Gunn, J.E., Uomoto, A., Roe, N., Schlegel, D., Rockosi, C.M., Carr, M.A., Leger, F., Dawson, K.S., Olmstead, M.D., Brinkmann, J., Owen, R., Barkhouser, R.H., Honscheid, K., Harding, P., Long, D., Lupton, R.H., Loomis, C., Anderson, L., Annis, J., Bernardi, M., Bhardwaj, V., Bizyaev, D., Bolton, A.S., Brewington, H., Briggs, J.W., Burles, S., Burns, J.G., Castander, F.J., Connolly, A., Davenport, J.R.A., Ebelke, G., Epps, H., Feldman, P.D., Friedman, S.D., Frieman, J., Heckman, T., Hull, C.L., Knapp, G.R., Lawrence, D.M., Loveday, J., Mannery, E.J., Malanushenko, E., Malanushenko, V., Merrelli, A.J., Muna, D., Newman, P.R., Nichol, R.C., Oravetz, D., Pan, K., Pope, A.C., Ricketts, P.G., Shelden, A., Sandford, D., Siegmund, W., Simmons, A., Smith, D.S., Snedden, S., Schneider, D.P., SubbaRao, M., Tremonti, C., Waddell, P., York, D.G.: The multi-object, fiber-fed spectrographs for the sloan digital sky survey and the Baryon oscillation spectroscopic survey. AJ **146**(2), 32 (2013). https://doi.org/10.1088/0004-6256/146/2/32
9. Lewis, I.J., Cannon, R.D., Taylor, K., Glazebrook, K., Bailey, J.A., Baldry, I.K., Barton, J.R., Bridges, T.J., Dalton, G.B., Farrell, T.J., Gray, P.M., Lankshear, A., McCowage, C., Parry, I.R., Sharples, R.M., Shortridge, K., Smith, G.A., Stevenson, J., Straede, J.O., Waller, L.G., Whittard, J.D., Wilcox, J.K., Willis, K.C.: The Anglo-Australian observatory 2dF facility. MNRAS **333**(2), 279–299 (2002). https://doi.org/10.1046/j.1365-8711.2002.05333.x
10. Parker, Q.A., Watson, F.G., Miziarski, S.: 6dF: An automated multi-object fiber spectroscopy system for the UKST. In: Arribas, S., Mediavilla, E., Watson, F. (eds.) Fiber optics in astronomy III. Astronomical Society of the Pacific Conference Series, vol. 152, p. 80 (1998)
11. Kimura, M., Maihara, T., Iwamuro, F., Akiyama, M., Tamura, N., Dalton, G.B., Takato, N., Tait, P., Ohta, K., Eto, S., Mochida, D., Elms, B., Kawate, K., Kurakami, T., Moritani, Y., Noumaru, J., Ohshima, N., Sumiyoshi, M., Yabe, K., Brzeski, J., Farrell, T., Frost, G., Gillingham, P.R., Haynes, R., Moore, A.M., Muller, R., Smedley, S., Smith, G., Bonfield, D.G., Brooks, C.B., Holmes, A.R., Curtis Lake, E., Lee, H., Lewis, I.J., Froud, T.R., Tosh, I.A., Woodhouse, G.F., Blackburn, C., Content, R., Dipper, N., Murray, G., Sharples, R., Robertson, D.J.: Fibre Multi-Object Spectrograph (FMOS) for the Subaru telescope. PASJ **62**, 1135–1147 (2010). https://doi.org/10.1093/pasj/62.5.1135
12. Cui, X.-Q., Zhao, Y.-H., Chu, Y.-Q., Li, G.-P., Li, Q., Zhang, L.-P., Su, H.-J., Yao, Z.-Q., Wang, Y.-N., Xing, X.-Z., Li, X.-N., Zhu, Y.-T., Wang, G., Gu, B.-Z., Luo, A.-L., Xu, X.-Q., Zhang, Z.-C., Liu, G.-R., Zhang, H.-T., Yang, D.-H., Cao, S.-Y., Chen, H.-Y., Chen, J.-J., Chen, K.-X., Chen, Y., Chu, J.-R., Feng, L., Gong, X.-F., Hou, Y.-H., Hu, H.-Z., Hu, N.-S., Hu, Z.-W., Jia, L., Jiang, F.-H., Jiang, X., Jiang, Z.-B., Jin, G., Li, A.-H., Li, Y., Li, Y.-P., Liu, G.-Q., Liu, Z.-G., Lu, W.-Z., Mao, Y.-D., Men, L., Qi, Y.-J., Qi, Z.-X., Shi, H.-M., Tang, Z.-H., Tao, Q.-S., Wang, D.-Q., Wang, D., Wang, G.-M., Wang, H., Wang, J.-N., Wang, J., Wang, J.-L., Wang, J.-P., Wang, L., Wang, S.-Q., Wang, Y., Wang, Y.-F., Xu, L.-Z., Xu, Y., Yang, S.-H., Yu, Y., Yuan, H., Yuan, X.-Y., Zhai, C., Zhang, J., Zhang, Y.-X., Zhang, Y., Zhao, M., Zhou, F., Zhou, G.-H., Zhu, J., Zou, S.-C.: The large sky area multi-object fiber spectroscopic telescope (LAMOST). Res. Astron. Astrophys. **12**(9), 1197–1242 (2012). https://doi.org/10.1088/1674-4527/12/9/003

13. Cirasuolo, M., Afonso, J., Carollo, M., Flores, H., Maiolino, R., Oliva, E., Paltani, S., Vanzi, L., Evans, C., Abreu, M., Atkinson, D., Babusiaux, C., Beard, S., Bauer, F., Bellazzini, M., Bender, R., Best, P., Bezawada, N., Bonifacio, P., Bragaglia, A., Bryson, I., Busher, D., Cabral, A., Caputi, K., Centrone, M., Chemla, F., Cimatti, A., Cioni, M.-R., Clementini, G., Coelho, J., Crnojevic, D., Daddi, E., Dunlop, J., Eales, S., Feltzing, S., Ferguson, A., Fisher, M., Fontana, A., Fynbo, J., Garilli, B., Gilmore, G., Glauser, A., Guinouard, I., Hammer, F., Hastings, P., Hess, A., Ivison, R., Jagourel, P., Jarvis, M., Kaper, L., Kauffman, G., Kitching, A.T., Lawrence, A., Lee, D., Lemasle, B., Licausi, G., Lilly, S., Lorenzetti, D., Lunney, D., Maiolino, R., Mannucci, F., McLure, R., Minniti, D., Montgomery, D., Muschielok, B., Nandra, K., Navarro, R., Norberg, P., Oliver, S., Origlia, L., Padilla, N., Peacock, J., Pedichini, F., Peng, J., Pentericci, L., Pragt, J., Puech, M., Randich, S., Rees, P., Renzini, A., Ryde, N., Rodrigues, M., Roseboom, I., Royer, F., Saglia, R., Sanchez, A., Schiavon, R., Schnetler, H., Sobral, D., Speziali, R., Sun, D., Stuik, R., Taylor, A., Taylor, W., Todd, S., Tolstoy, E., Torres, M., Tosi, M., Vanzella, E., Venema, L., Vitali, F., Wegner, M., Wells, M., Wild, V., Wright, G., Zamorani, G., Zoccali, M.: MOONS: The multi-object optical and near-infrared spectrograph for the VLT. In: Ramsay, S.K., McLean, I.S., Takami, H. (eds.) Ground-based and airborne instrumentation for astronomy V. Society of photo-optical instrumentation engineers (SPIE) conference series, vol. 9147, p. 91470 (2014). https://doi.org/10.1117/12.2056012
14. Tamura, N., Takato, N., Shimono, A., Moritani, Y., Yabe, K., Ishizuka, Y., Ueda, A., Kamata, Y., Aghazarian, H., Arnouts, S., Barban, G., Barkhouser, R.H., Borges, R.C., Braun, D.F., Carr, M.A., Chabaud, P.-Y., Chang, Y.-C., Chen, H.-Y., Chiba, M., Chou, R.C.Y., Chu, Y.-H., Cohen, J., de Almeida, R.P., de Oliveira, A.C., de Oliveira, L.S., Dekany, R.G., Dohlen, K., dos Santos, J.B., dos Santos, L.H., Ellis, R., Fabricius, M., Ferrand, D., Ferreira, D., Golebiowski, M., Greene, J.E., Gross, J., Gunn, J.E., Hammond, R., Harding, A., Hart, M., Heckman, T.M., Hirata, C.M., Ho, P., Hope, S.C., Hovland, L., Hsu, S.-F., Hu, Y.-S., Huang, P.-J., Jaquet, M., Jing, Y., Karr, J., Kimura, M., King, M.E., Komatsu, E., Le Brun, V., Le Fèvre, O., Le Fur, A., Le Mignant, D., Ling, H.-H., Loomis, C.P., Lupton, R.H., Madec, F., Mao, P., Marrara, L.S., Mendes de Oliveira, C., Minowa, Y., Morantz, C., Murayama, H., Murray, G.J., Ohyama, Y., Orndorff, J., Pascal, S., Pereira, J.M., Reiley, D., Reinecke, M., Ritter, A., Roberts, M., Schwochert, M.A., Seiffert, M.D., Smee, S.A., Sodre, L., Spergel, D.N., Steinkraus, A.J., Strauss, M.A., Surace, C., Suto, Y., Suzuki, N., Swinbank, J., Tait, P.J., Takada, M., Tamura, T., Tanaka, Y., Tresse, L., Verducci, O., Vibert, D., Vidal, C., Wang, S.-Y., Wen, C.-Y., Yan, C.-H., Yasuda, N.: Prime Focus Spectrograph (PFS) for the Subaru telescope: Overview, recent progress, and future perspectives. In: Evans, C.J., Simard, L., Takami, H. (eds.) Ground-based and airborne instrumentation for astronomy VI. Society of Photo-Optical Instrumentation Engineers (SPIE) Conference Series, vol. 9908, p. 99081 (2016). https://doi.org/10.1117/12.2232103
15. Meyer, R.D., Kearney, K.J., Ninkov, Z., Cotton, C.T., Hammond, P., Statt, B.D.: RITMOS: A micromirror-based multi-object spectrometer. In: Moorwood, A.F.M., Iye, M. (eds.) Ground-based instrumentation for astronomy. Society of Photo-Optical Instrumentation Engineers (SPIE) Conference Series, vol. 5492, pp. 200–219 (2004). https://doi.org/10.1117/12.549897
16. Zamkotsian, F., Spano, P., Lanzoni, P., Ramarijaona, H., Moschetti, M., Riva, M., Bon, W., Nicastro, L., Molinari, E., Cosentino, R., Ghedina, A., Gonzalez, M., Di Marcantonio, P., Coretti, I., Cirami, R., Zerbi, F., Valenziano, L.: BATMAN: A DMD-based multi-object spectrograph on Galileo telescope. In: Ramsay, S.K., McLean, I.S., Takami, H. (eds.) Ground-based and airborne instrumentation for astronomy V. Society of Photo-Optical Instrumentation Engineers (SPIE) Conference Series, vol. 9147, p. 914713 (2014). https://doi.org/10.1117/12.2055192
17. Smee, S.A., Barkhouser, R., Harding, A., Hope, S., Robberto, M., Ninkov, Z., Gennaro, M.: The opto-mechanical design of SAMOS: A DMD-based spectrograph for the SOAR telescope. In: Evans, C.J., Simard, L., Takami, H. (eds.) Ground-based and airborne instrumentation for astronomy VII. Society of Photo-Optical Instrumentation Engineers (SPIE) Conference Series, vol. 10702, p. 107021 (2018). https://doi.org/10.1117/12.2311876
18. MacKenty, J.W., Ohl, R.G. IV, Greenhouse, M.A., Green, R.F.: Commissioning of the IRMOS MEMS spectrometer. In: McLean, I.S., Iye, M. (eds.) Ground-based and airborne instrumentation for astronomy. Society of Photo-Optical Instrumentation Engineers (SPIE) Conference Series, vol. 6269, p. 626915 (2006). https://doi.org/10.1117/12.672317

19. Spanò, P., Zamkotsian, F., Content, R., Grange, R., Robberto, M., Valenziano, L., Zerbi, F.M., Sharples, R.M., Bortoletto, F., de Caprio, V., Martin, L., de Rosa, A., Franzetti, P., Diolaiti, E., Garilli, B., Guzzo, L., Leutenegger, P., Scodeggio, M., Vink, R., Zamorani, G., Cimatti, A.: DMD multi-object spectroscopy in space: The EUCLID study. In: MacEwen, H.A., Breckinridge, J.B. (eds.) UV/Optical/IR Space Telescopes: Innovative technologies and concepts IV. Society of Photo-Optical Instrumentation Engineers (SPIE) Conference Series, vol. 7436, p. 74360 (2009). https://doi.org/10.1117/12.825641
20. Cote, P., Abraham, B., Balogh, M., Capak, P., Carlberg, R., Cowan, N., Djazovski, O., Drissen, L., Drout, M., Dupuis, J., Evans, C., Fantin, N., Ferrarese, L., Fraser, W., Gallagher, S., Girard, T., Gleisinger, R., Grandmont, F., Hall, P., Hellmich, M., Hardy, T., Harrison, P., Hlozek, R., Haggard, D., Henault-Brunet, V., Hutchings, J., Khatu, V., Kavelaars, J., Laurin, D., Lavigne, J.-F., Lisman, D., Marois, C., McCabe, D., Metchev, S., Moutard, T., Netterfield, B., Nikzad, S., Ouellette, N., Pass, E., Parker, L., Pazder, J., Percival, W., Rhodes, J., Robert, C., Rowe, J., Sanchez-Janssen, R., Sivakoff, G., Shapiro, C., Sawicki, M., Scott, A., Van Waerbeke, L., Venn, K.: CASTOR: A flagship canadian space telescope. In: Canadian long range plan for astronomy and astrophysics white papers, vol. 2020, p. 18 (2019). https://doi.org/10.5281/zenodo.3758463
21. Content, R., Wang, Y., Robberto, M., Dickinson, M., Ferguson, H., Hillenbrand, L., Fraser, W., Behroozi, P., Brinchmann, J., Cimatti, A., Daddi, E., Hirata, C., Hudson, M., Kirkpatrick, J.D., Barkhouser, R., Bartlett, J., Benjamin, R., Chary, R., Conroy, C., Donahue, M., Doré, O., Eisenhardt, P., Glazebrook, K., Helou, G., Malhotra, S., Moscardini, L., Ninkov, Z., Orsi, A., Ressler, M., Rhoads, J., Rhodes, J., Shapley, A., Smee, S.: ATLAS probe for the study of galaxy evolution with 300,000,000 galaxy spectra. In: Lystrup, M., MacEwen, H.A., Fazio, G.G., Batalha, N., Siegler, N., Tong, E.C. (eds.) Space telescopes and instrumentation 2018: Optical, infrared, and millimeter wave. Society of Photo-Optical Instrumentation Engineers (SPIE) Conference Series, vol. 10698, p. 106980 (2018). https://doi.org/10.1117/12.2313082
22. Content, R., Wang, Y., Robberto, M., Armus, L., Beutler, F., Bolzonella, M., Brieden, S., Brinchmann, J., Daddi, E., Dickinson, M., Faisst, A., Hillenbrand, L., Howlett, C., Kartaltepe, J., Koeppe, D., Lawrence, J., Mei, S., Mueller, E.-M., Nadathur, S., Ninkov, Z., Osato, K., Papovich, C., Percival, W., Piotrowski, J., Pozzetti, L., Raccanelli, A., Rhodes, J., Saito, S., Smee, S., Vorobiev, D., Zemcov, M.: SIRMOS: NIR spectroscopy of 131,000,000 galaxies over $1 < z < 4$ and R 1300. In: Coyle, L.E., Matsuura, S., Perrin, M.D. (eds.) Space telescopes and instrumentation 2024: Optical, infrared, and millimeter wave. Society of Photo-Optical Instrumentation Engineers (SPIE) Conference Series, vol. 13092, p. 130920 (2024). https://doi.org/10.1117/12.3017865
23. Halferty, G., Vorobiev, D., Fleming, B., Chafetz, D., Williams, J.: Design of the spectroscopic ultraviolet multi-object observatory (SUMO) prototype for deployment on the INFUSE sounding rocket. In: Siegmund, O.H., Hoadley, K. (eds.) UV, x-ray, and gamma-ray space instrumentation for astronomy XXIII. Society of Photo-Optical Instrumentation Engineers (SPIE) Conference Series, vol. 12678, p. 126780 (2023). https://doi.org/10.1117/12.2676544
24. Zamkotsian, F., Lanzoni, P., Grassi, E., Barette, R., Fabron, C., Tangen, K., Valenziano, L., Marchand, L., Duvet, L.: Successful evaluation for space applications of the 2048×1080 DMD. In: Douglass, M.R., Oden, P.I. (eds.) Society of Photo-Optical Instrumentation Engineers (SPIE) conference series. Society of Photo-Optical Instrumentation Engineers (SPIE) Conference Series, vol. 7932, p. 79320 (2011). https://doi.org/10.1117/12.876872
25. Fourspring, K., Ninkov, Z., Fodness, B.C., Robberto, M., Heap, S., Kim, A.G.: Proton radiation testing of digital micromirror devices for space applications. Opt. Eng. **52**, 091807 (2013). https://doi.org/10.1117/1.OE.52.9.091807
26. Oram, K., Vorobiev, D., Ninkov, Z., Irwin, A., Pellish, J.A., Carts, M., Brown, S.K.: The effects of gamma radiation on digital micromirror devices. In: Douglass, M.R., Ehmke, J., Lee, B.L. (eds.) Emerging digital micromirror device based systems and applications XI. Society of Photo-Optical Instrumentation Engineers (SPIE) Conference Series, vol. 10932, p. 109320 (2019). https://doi.org/10.1117/12.2508935
27. Vorobiev, D., Travinsky, A., Raisanen, A.D., Ninkov, Z., Schwartz, T.A., Robberto, M., Heap, S.: Shock and vibration testing of digital micromirror devices (DMDs) for space-based applications. In: Navarro, R., Burge, J.H. (eds.) Advances in optical and mechanical technologies for telescopes and instrumentation II. Society of Photo-Optical Instrumentation Engineers (SPIE) Conference Series, vol. 9912, p. 99125 (2016). https://doi.org/10.1117/12.2233591

28. Travinsky, A., Vorobiev, D., Ninkov, Z., Raisanen, A., Quijada, M.A., Smee, S.A., Pellish, J.A., Schwartz, T., Robberto, M., Heap, S., Conley, D., Benavides, C., Garcia, N., Bredl, Z., Yllanes, S.: Evaluation of digital micromirror devices for use in space-based multiobject spectrometer application. J. Astron. Telescopes Instrum. Syst. **3**, 035003 (2017). https://doi.org/10.1117/1.JATIS.3.3.035003
29. Vorobiev, D., Fleming, B., Oram, K.V., Chafetz, D., Zimmer, P., Irwin, A., Del Hoyo, J., Quijada, M., Ninkov, Z.: Far-UV multi-object spectroscopy with digital micromirror devices (DMDs). In: den Herder, J.-W.A., Nikzad, S., Nakazawa, K. (eds.) Society of Photo-Optical Instrumentation Engineers (SPIE) conference series. Society of Photo-Optical Instrumentation Engineers (SPIE) Conference Series, vol. 11444, p. 114446 (2021). https://doi.org/10.1117/12.2562540
30. Singh, K.P., Tandon, S.N., Agrawal, P.C., Antia, H.M., Manchanda, R.K., Yadav, J.S., Seetha, S., Ramadevi, M.C., Rao, A.R., Bhattacharya, D., Paul, B., Sreekumar, P., Bhattacharyya, S., Stewart, G.C., Hutchings, J., Annapurni, S.A., Ghosh, S.K., Murthy, J., Pati, A., Rao, N.K., Stalin, C.S., Girish, V., Sankarasubramanian, K., Vadawale, S., Bhalerao, V.B., Dewangan, G.C., Dedhia, D.K., Hingar, M.K., Katoch, T.B., Kothare, A.T., Mirza, I., Mukerjee, K., Shah, H., Shah, P., Mohan, R., Sangal, A.K., Nagabhusana, S., Sriram, S., Malkar, J.P., Sreekumar, S., Abbey, A.F., Hansford, G.M., Beardmore, A.P., Sharma, M.R., Murthy, S., Kulkarni, R., Meena, G., Babu, V.C., Postma, J.: ASTROSAT mission. In: Takahashi, T., den Herder, J.-W.A., Bautz, M. (eds.) Space telescopes and instrumentation 2014: ultraviolet to gamma ray. Society of Photo-Optical Instrumentation Engineers (SPIE) Conference Series, vol. 9144, p. 91441 (2014). https://doi.org/10.1117/12.2062667
31. Kumar, A., Ghosh, S.K., Hutchings, J., Kamath, P.U., Kathiravan, S., Mahesh, P.K., Murthy, J., Nagbhushana, S., Pati, A.K., Rao, M.N., Rao, N.K., Sriram, S., Tandon, S.N.: Ultra Violet Imaging Telescope (UVIT) on ASTROSAT. In: Takahashi, T., Murray, S.S., den Herder, J.-W.A. (eds.) Space telescopes and instrumentation 2012: Ultraviolet to gamma ray. Society of Photo-Optical Instrumentation Engineers (SPIE) Conference Series, vol. 8443, p. 84431 (2012). https://doi.org/10.1117/12.924507
32. Girish, V., Tandon, S.N., Sriram, S., Kumar, A., Postma, J.: Mapping distortion of detectors in uvit onboard astrosat observatory. Exp. Astron. **43**(1), 59–74 (2017). https://doi.org/10.1007/s10686-016-9520-3
33. Kathiravan, S., Tandon, S.N., Raghavendra Prasad, B., Sriram, S., Pradeep, A., Vishnu, T., Mahesh, P.K., Kamath, P.U., Nagabhushana, S., Kumar, A.: Contamination control of UVIT. J. Astrophys. Astron. **42**(2), 41 (2021). https://doi.org/10.1007/s12036-020-09681-4
34. Tandon, S.N., Subramaniam, A., Girish, V., Postma, J., Sankarasubramanian, K., Sriram, S., Stalin, C.S., Mondal, C., Sahu, S., Joseph, P., Hutchings, J., Ghosh, S.K., Barve, I.V., George, K., Kamath, P.U., Kathiravan, S., Kumar, A., Lancelot, J.P., Leahy, D., Mahesh, P.K., Mohan, R., Nagabhushana, S., Pati, A.K., Kameswara Rao, N., Sreedhar, Y.H., Sreekumar, P.: In-orbit calibrations of the ultraviolet imaging telescope. AJ **154**(3), 128 (2017). https://doi.org/10.3847/1538-3881/aa8451
35. Subramaniam, A., Tandon, S.N., Hutchings, J., Ghosh, S.K., George, K., Girish, V., Kamath, P.U., Kathiravan, S., Kumar, A., Lancelot, J.P., Mahesh, P.K., Mohan, R., Murthy, J., Nagabhushana, S., Pati, A.K., Postma, J., Rao, N.K., Sankarasubramanian, K., Sreekumar, P., Sriram, S., Stalin, C.S., Sutaria, F., Sreedhar, Y.H., Barve, I.V., Mondal, C., Sahu, S.: In-orbit performance of UVIT on ASTROSAT. In: den Herder, J.-W.A., Takahashi, T., Bautz, M. (eds.) Space telescopes and instrumentation 2016: Ultraviolet to gamma ray. Society of Photo-Optical Instrumentation Engineers (SPIE) Conference Series, vol. 9905, p. 99051 (2016). https://doi.org/10.1117/12.2235271
36. Tandon, S.N., Postma, J., Joseph, P., Devaraj, A., Subramaniam, A., Barve, I.V., George, K., Ghosh, S.K., Girish, V., Hutchings, J.B., Kamath, P.U., Kathiravan, S., Kumar, A., Lancelot, J.P., Leahy, D., Mahesh, P.K., Mohan, R., Nagabhushana, S., Pati, A.K., Rao, N.K., Sankarasubramanian, K., Sriram, S., Stalin, C.S.: Additional calibration of the ultraviolet imaging telescope on board AstroSat. AJ **159**(4), 158 (2020). https://doi.org/10.3847/1538-3881/ab72a3
37. Subramaniam, A.: An overview of the proposed Indian spectroscopic and imaging space telescope. J. Astrophys. Astron. **43**(2), 80 (2022). https://doi.org/10.1007/s12036-022-09870-3
38. Sriram, S., Valsan, V., Subramaniam, A., Unni, C.V., Maheswar, G., Chand, T.: Indian spectroscopic and imaging space telescope (INSIST): An optics design trade-off study. J. Astrophys. Astron. **44**(2), 55 (2023). https://doi.org/10.1007/s12036-023-09934-y
39. Sriram, S., Valsan, V., Hoodati, A., Subramaniam, A., Maheswar, G.: DMD based multi-object spectrograph for Indian spectroscopic and imaging space telescope: INSIST. J. Astron. Instrum. **12**(4), 2350012 (2023). https://doi.org/10.1142/S2251171723500125
40. Texas Instruments: DMD DLP9500 datasheet. https://datasheet.octopart.com/DLP9500FLN-Texas-Instruments-datasheet-12084505.pdf. DLP 0.95 1080p 2x LVDS Type A DMD (2012)
41. Prieto-Blanco, X., Montero-Orille, C., Couce, B., de la Fuente, R.: Analytical design of an Offner imaging spectrometer. Opt. Express **14**(20), 9156–9168 (2006). https://doi.org/10.1364/OE.14.009156

42. Piotrowski, J.J., Smee, S.A., Hope, S., Robberto, M.: In-situ evaluation of DMD contrast ratio using SAMOS: A DMD-based multi-object spectrograph and imager. In: Bryant, J.J., Motohara, K., Vernet, J.R.D. (eds.) Ground-based and airborne instrumentation for astronomy X. Society of Photo-Optical Instrumentation Engineers (SPIE) Conference Series, vol. 13096, p. 13096 (2024). https://doi.org/10.1117/12.3020820
43. Vorobiev, D., Travinsky, A., Quijada, M.A., Ninkov, Z., Raisanen, A.D., Robberto, M., Heap, S.: Measurements of the reflectance, contrast ratio, and scattering properties of digital micromirror devices (DMDs). In: Navarro, R., Burge, J.H. (eds.) Advances in optical and mechanical technologies for telescopes and instrumentation II. Society of Photo-Optical Instrumentation Engineers (SPIE) Conference Series, vol. 9912, p. 99125 (2016). https://doi.org/10.1117/12.2233638
44. Tody, D.: The IRAF data reduction and analysis system. In: Crawford, D.L. (ed.) Instrumentation in astronomy VI. Society of Photo-Optical Instrumentation Engineers (SPIE) Conference Series, vol. 627, p. 733 (1986). https://doi.org/10.1117/12.968154
45. Harris, C.R., Millman, K.J., Walt, S.J., Gommers, R., Virtanen, P., Cournapeau, D., Wieser, E., Taylor, J., Berg, S., Smith, N.J., Kern, R., Picus, M., Hoyer, S., Kerkwijk, M.H., Brett, M., Haldane, A., Río, J.F., Wiebe, M., Peterson, P., Gérard-Marchant, P., Sheppard, K., Reddy, T., Weckesser, W., Abbasi, H., Gohlke, C., Oliphant, T.E.: Array programming with NumPy. Nature **585**(7825), 357–362 (2020). https://doi.org/10.1038/s41586-020-2649-2
46. Astropy Collaboration, Price-Whelan, A.M., Lim, P.L., Earl, N., Starkman, N., Bradley, L., Shupe, D.L., Patil, A.A., Corrales, L., Brasseur, C.E., Nöthe, M., Donath, A., Tollerud, E., Morris, B.M., Ginsburg, A., Vaher, E., Weaver, B.A., Tocknell, J., Jamieson, W., van Kerkwijk, M.H., Robitaille, T.P., Merry, B., Bachetti, M., Günther, H.M., Aldcroft, T.L., Alvarado-Montes, J.A., Archibald, A.M., Bódi, A., Bapat, S., Barentsen, G., Bazán, J., Biswas, M., Boquien, M., Burke, D.J., Cara, D., Cara, M., Conroy, K.E., Conseil, S., Craig, M.W., Cross, R.M., Cruz, K.L., D'Eugenio, F., Dencheva, N., Devillepoix, H.A.R., Dietrich, J.P., Eigenbrot, A.D., Erben, T., Ferreira, L., Foreman-Mackey, D., Fox, R., Freij, N., Garg, S., Geda, R., Glattly, L., Gondhalekar, Y., Gordon, K.D., Grant, D., Greenfield, P., Groener, A.M., Guest, S., Gurovich, S., Handberg, R., Hart, A., Hatfield-Dodds, Z., Homeier, D., Hosseinzadeh, G., Jenness, T., Jones, C.K., Joseph, P., Kalmbach, J.B., Karamehmetoglu, E., Kałuszyński, M., Kelley, M.S.P., Kern, N., Kerzendorf, W.E., Koch, E.W., Kulumani, S., Lee, A., Ly, C., Ma, Z., MacBride, C., Maljaars, J.M., Muna, D., Murphy, N.A., Norman, H., O'Steen, R., Oman, K.A., Pacifici, C., Pascual, S., Pascual-Granado, J., Patil, R.R., Perren, G.I., Pickering, T.E., Rastogi, T., Roulston, B.R., Ryan, D.F., Rykoff, E.S., Sabater, J., Sakurikar, P., Salgado, J., Sanghi, A., Saunders, N., Savchenko, V., Schwardt, L., Seifert-Eckert, M., Shih, A.Y., Jain, A.S., Shukla, G., Sick, J., Simpson, C., Singanamalla, S., Singer, L.P., Singhal, J., Sinha, M., Sipőcz, B.M., Spitler, L.R., Stansby, D., Streicher, O., Šumak, J., Swinbank, J.D., Taranu, D.S., Tewary, N., Tremblay, G.R., de Val-Borro, M., Van Kooten, S.J., Vasović, Z., Verma, S., de Miranda Cardoso, J.V., Williams, P.K.G., Wilson, T.J., Winkel, B., Wood-Vasey, W.M., Xue, R., Yoachim, P., Zhang, C., Zonca, A., Astropy Project Contributors: The Astropy Project: Sustaining and growing a community-oriented open-source project and the latest major release (v5.0) of the core package. APJ **935**(2), 167 (2022). https://doi.org/10.3847/1538-4357/ac7c74
47. Virtanen, P., Gommers, R., Oliphant, T.E., Haberland, M., Reddy, T., Cournapeau, D., Burovski, E., Peterson, P., Weckesser, W., Bright, J., van der Walt, S.J., Brett, M., Wilson, J., Millman, K.J., Mayorov, N., Nelson, A.R.J., Jones, E., Kern, R., Larson, E., Carey, C.J., Polat, İ., Feng, Y., Moore, E.W., VanderPlas, J., Laxalde, D., Perktold, J., Cimrman, R., Henriksen, I., Quintero, E.A., Harris, C.R., Archibald, A.M., Ribeiro, A.H., Pedregosa, F., van Mulbregt, P., SciPy 1.0 Contributors: SciPy 1.0: Fundamental algorithms for scientific computing in Python. Nat. Methods **17**, 261–272 (2020). https://doi.org/10.1038/s41592-019-0686-2
48. Hunter, J.D.: Matplotlib: A 2d graphics environment. Comput. Sci. Eng. **9**(3), 90–95 (2007). https://doi.org/10.1109/MCSE.2007.55
49. Zemax, LLC: Zemax OpticStudio. (2014). Available at https://www.zemax.com/
50. Solidworks: SOLIDWORKS 2024 (2024). https://www.solidworks.com/
51. Autodesk, Inc.: AutoCAD. (2024). Available at https://www.autodesk.com/products/autocad